bioRxiv preprint doi: https://doi.org/10.1101/744763; this version posted September 12, 2019. The copyright holder for this preprint (which was not certified by peer review) is the author/funder. All rights reserved. No reuse allowed without permission.

NRP2 as an emerging angiogenic player; promoting endothelial cell adhesion and migration by regulating recycling of α5 integrin.

Authors: Abdullah AA Alghamdi[1,2,*], Christopher J Benwell[3,*], Samuel J Atkinson[1,4], Jordi Lambert[5], and Stephen D Robinson[1,3]

Author Affiliations:

[1]School of Biological Sciences, University of East Anglia, Norwich Research Park, Norwich, UK.

[2]Current affiliation: Department of Biology, Faculty of Science, Albaha University, Albaha, Saudi Arabia.

[3]Gut Microbes and Health, Quadram Institute Bioscience, Norwich Research Park, Norwich, UK.

[4]Current affiliation: Cancer Research UK Beatson Institute, Glasgow, UK.

[5]Faculty of Medicine and Health Sciences, University of East Anglia, Norwich Research Park, Norwich, UK.

[*]contributed equally to this work

Keywords

Neuropilins, endothelium, integrins, protein trafficking

bioRxiv preprint doi: https://doi.org/10.1101/744763; this version posted September 12, 2019. The copyright holder for this preprint (which was not certified by peer review) is the author/funder. All rights reserved. No reuse allowed without permission.

Abstract

Angiogenesis relies on the ability of endothelial cells (ECs) to migrate over the extracellular matrix via integrin receptors to respond to an angiogenic stimulus. Of the two neuropilin (NRP) orthologs to be identified, both have been reported to be expressed on normal blood and lymphatic ECs, and to play roles in the formation of blood and lymphatic vascular networks during angiogenesis. Whilst the role of NRP1 and its interactions with integrins during angiogenesis has been widely studied, the role of NRP2 in ECs is poorly understood. Here we demonstrate that NRP2 promotes EC adhesion and migration over fibronectin (FN) matrices in a mechanistically distinct fashion to NRP1, showing no dependence on β3 integrin (ITGB3) expression, or VEGF stimulation. Furthermore, we highlight evidence of a regulatory crosstalk between NRP2 and α5 integrin (ITGA5) in ECs, with NRP2 depletion eliciting an upregulation of ITGA5 expression and disruptions in ITGA5 cellular organisation. Finally, we propose a mechanism whereby NRP2 regulates ITGA5 trafficking in ECs by promoting Rab11-dependent recycling of ITGA5. NRP2 depleted ECs were found to exhibit reduced levels of total ITGA5 subunit recycling compared to wild-type (WT) ECs, where we demonstrate a strong co-localisation between NRP2, ITGA5 and Rab11. Our findings expose NRP2 as a novel angiogenic player by promoting ITGA5-mediated EC adhesion and migration on FN.

Introduction

Neuropilins (NRPs) are single non-tyrosine kinase receptors belonging to a family of type I transmembrane glycoproteins (MW ~130–140 kDa) [1]. To date, two NRP orthologs have been identified in vertebrates, NRP1 and NRP2, both of which share a very similar domain structure and an overall 44% amino acid homology [2], [3]. Their expression and function have been identified in many cell types, including nerve cells, endothelial cells (ECs), epithelial cells, immune cells, osteoblasts and tumour cells [3], [4]. In ECs, it is believed that NRPs play an essential role in sprouting angiogenesis and lymphogenesis through the selective binding to members of the vascular endothelial growth factor (VEGF) family. Following this complex formation, NRPs function as co-receptors with VEGFRs to enhance the VEGF-induced activation of many intracellular pathways [5]. As such, NRP functions have been implicated in influencing cell adhesion, migration and permeability during angiogenesis, under both physiological and pathological conditions [6], [7], [8]. Studies have, however, provided evidence to suggest that NRPs can mediate ligand signalling independently of VEGFRs, in addition to regulating VEGFRs independently of VEGF binding.

Based on early transgenic mouse studies in this field, it was originally speculated that NRP1 is mainly expressed on arteries, arterioles and capillaries, whereas NRP2 is expressed on veins, venules and lymphatic vessels [9], [10]. However, subsequent studies have revealed that both NRPs are expressed in normal blood and lymphatic endothelial cells, and both play essential roles in forming blood and lymphatic vasculature networks [11], [12], [13]. Despite this, investigations into elucidating the roles of endothelial NRPs during angiogenesis have, for the most part, focused on NRP1 [3]. With regard to NRP2, studies have instead focused on annotating a role in cancer cells, where its upregulation is consistent with cancer progression in a number of cell types (e.g. neuroblastomas [14], non-small cell lung carcinoma [NSCLC] [15], human prostate carcinoma, melanoma [4], lung cancer [16], [15], [17], myeloid leukaemia [18], breast cancer [19] and pancreatic cancer [20]). Interestingly, Favier *et al.* recapitulated this upregulation of NRP2 observed in cancer cells by

bioRxiv preprint doi: https://doi.org/10.1101/744763; this version posted September 12, 2019. The copyright holder for this preprint (which was not certified by peer review) is the author/funder. All rights reserved. No reuse allowed without permission.

overexpressing NRP2 in human microvascular ECs (hMVECs), and found that cell survival in these ECs was significantly increased following stimulation with either VEGF-A- or VEGF-C. Furthermore, NRP2 knockdown significantly inhibited both VEGF-A- and VEGF-C-induced migration, suggesting that NRP2 as a potential pharmacological target. Crucially, Favier *et al.* highlighted the importance of understanding the cross-talk between NRP2 and other receptors (mainly VEGF, integrins and plexins) in ECs, which will aid in the design of novel drugs to better control the mechanisms underlying angiogenesis and lymph-angiogenesis in autoimmune diseases and tumour development [21].

We have previously described a link between NRP1 and the β3-integrin (ITGB3) subunit during VEGF-induced angiogenesis. We reported that complete loss of the *Itgb3* gene enhanced EC permeability through the upregulation of VEGF-VEGFR2-ERK1/2 signalling [22], and that NRP1 and ERK1/2 expression was elevated in ITGB3-NULL ECs. Subsequent targeting of NRP1 in ITGB3-NULL mice revealed a significant inhibition of VEGF-induced angiogenesis compared to WT mice, indicating that the elevation of angiogenesis in the absence of the *Itgb3* gene is dependent on NRP1 expression [23], [8]. In this study we aimed to investigate whether NRP2 shared a similar interaction with ITGB3 in the context of angiogenesis.

Results

NRP2 function is not regulated by ITGB3 during VEGFR2-mediated signalling or migration over FN

We previously showed the involvement of NRP1 during VEGF-stimulated angiogenesis to be dependent upon ITGB3 in ECs [8]. Due to the structural homology between NRP1 and NRP2 [3], we decided to first consider whether, like NRP1, NRP2's function shares a dependency on ITGB3 during VEGF-mediated angiogenic responses in ECs. To investigate this, we isolated mouse lung microvascular endothelial cells (mLMECs) from both wild-type (WT) and ITGB3-heterozygous (β3HET) mice and immortalised them with polyoma-middle-T-antigen (PyMT) by retroviral transduction. DNA was extracted from multiple immortalised lines, and analysed by PCR to confirm their genetic status as either WT or β3HET cells (**Suppl. Fig1A**). We subsequently confirmed the EC identity of each immortalised line by examining the expression of EC markers including VE-Cadherin [24], [25], in addition to quantifying the expression of ITGB3 in β3HET ECs. Each clone was confirmed to express VE-Cadherin, and all β3HET ECs were confirmed to express approximately 50% ITGB3 compared to their WT counterparts (**Suppl. Fig1B-C**). We reported previously that in β3HET ECs, NRP1 expression is upregulated. In addition, NRP1 appeared only to play a role in post development angiogenesis when ITGB3 expression is reduced [8]. Western blot quantification of NRP2 expression between WT and β3HET protein lysates showed a similar elevation in NRP2 expression in β3HET ECs (**Fig1A**), suggesting the existence of a regulatory nexus between NRP2 and ITGB3, which warranted further exploration.

As NRP2 has been shown to regulate VEGF-induced signalling in both human lymphatic [26], and lymphatic microvascular ECs, we examined whether NRP2 regulates pro-angiogenic signalling responses to VEGF and if the effects are dependent on ITGB3. Using a 90% efficient NRP2 specific siRNA (**Suppl. Fig1D**) versus a control siRNA transfected into our WT and β3HET ECs, we measured differences in VEGFR2 and ERK phosphorylation over a timecourse of 15 minutes. We observed only marginally attenuated VEGFR2 and ERK

bioRxiv preprint doi: https://doi.org/10.1101/744763; this version posted September 12, 2019. The copyright holder for this preprint (which was not certified by peer review) is the author/funder. All rights reserved. No reuse allowed without permission.

phosphorylation by Western blot analysis in response to NRP2 silencing and saw no differences between WT and β3HET ECs (**Fig1B**), suggesting that ITGB3 does not regulate NRP2 dependent VEGF induced signalling in our cells.

To explore the possibility of a regulatory axis between NRP2 and ITGB3 further, we examined cellular migration. Angiogenesis relies on the ability of ECs to respond to angiogenic stimuli by migrating over an extracellular matrix (ECM). We have shown previously that NRP1 plays a role in promoting EC migration over fibronectin (FN) matrices, but only when ITGB3 levels are reduced [8]. Independent studies have also described NRP2 silencing to inhibit VEGF-induced migration of human microvascular ECs [21] and human lymphatic ECs [26]. We therefore chose to examine the effects of NRP2 depletion on EC migration over FN in our mLMECs, and to determine whether any effect is dependent upon ITGB3 expression. To achieve this, control and NRP2 siRNA transfected WT and β3HET ECs were plated on FN and random migration speed was measured by timelapse microscopy over 15 hours. As previously reported, we observed β3HET ECs to migrate faster over a FN matrix than WT ECs. However, unlike NRP1, depletion of NRP2 significantly reduced EC migration speed, but independently of ITGB3 expression (**Fig1C**). We therefore conclude that ITGB3 does not regulate NRP2 function during these angiogenic processes. Note, whilst NRP2 regulated overall cell migration, we saw no changes in directionality (not shown).

Depletion of NRP2 in ECs disrupts adhesion to FN matrices

Whilst the upregulation of NRP2 expression we observe in β3HET ECs suggests a regulatory crosstalk between NRP2 and ITGB3 (**Fig1A**), NRP2 regulated signalling and migration show no dependence on ITGB3. As NRP2 depletion significantly impaired the ability for ECs to migrate over FN (**Fig1C**), but not to undergo proliferation (**Suppl. Fig2A**) we chose to examine whether NRP2 plays a role in focal adhesion (FA) turnover. Migration is dependent on the ability of cells to adhere to a matrix via the formation of FA complexes that continuously cycle through phases of assembly and disassembly. FAs comprise a module of recruited intracellular proteins, including integrins, that link to the actin cytoskeleton to mediate mechanical changes in the cell [27], [28], [29], [30]. FA assembly and disassembly was monitored in ECs treated with either control or NRP2 siRNAs, transfected with paxillin-GFP, by timelapse microscopy for 30 minutes over a FN matrix. Silencing of NRP2 in mLMECs significantly reduced the rate of both FA assembly and disassembly compared to control siRNA treated cells (**Fig2A**). We also measured FA number and size distribution in ECs by immunolabelling for endogenous paxillin in cells that had adhered to FN for 90 minutes, a time that allows mature FAs to form [31], [32], [33]. Despite no significant difference in average cell area (**Suppl. Fig2B**), FAs were significantly fewer in number and smaller in average size in NRP2 siRNA treated cells compared to control siRNA treated ECs (**Fig2B**), suggesting NRP2 depletion inhibits FA maturation.

Given the observed disruption in FA dynamics upon NRP2 silencing, and knowing signals from FAs can influence cytoskeletal organisation and actin polymerisation, and cytoskeletal structures in turn influence the formation and disassembly of FAs, we next examined whether NRP2 knockdown resulted in: (1) morphological changes to the actin cytoskeleton; and (2) changes in adhesion to FN. Phalloidin staining of F-actin revealed NRP2 siRNA treated ECs adhered to FN for either 90 or 180 minutes exhibited a rounded morphology with visibly fewer stress fibres, and localisation of actin fibres to rings at the cell periphery compared to control siRNA treated ECs (**Fig2C**). This phenotype is characteristic of low motility, and is reminiscent of that observed by Fantin et al. in hMVECs following NRP1 knockdown, in

bioRxiv preprint doi: https://doi.org/10.1101/744763; this version posted September 12, 2019. The copyright holder for this preprint (which was not certified by peer review) is the author/funder. All rights reserved. No reuse allowed without permission.

addition to a significantly reduced number of actin positive, filopodia-like microspikes [34]. Finally, to directly assess how these changes to FAs and the actin cytoskeleton might affect the ability of mLMECs to adhere to FN, we compared the relative number of cells adhered to 96-well plates pre-coated with FN for either 15 or 30 minutes. At both timepoints significantly fewer cells adhered to FN following NRP2 siRNA treatment compared to control siRNA treated ECs (**Fig2D**), suggesting that NRP2 promotes both adhesion and migration on FN matrices by regulating both FA and actin cytoskeletal dynamics.

NRP2 regulates ITGA5 expression in ECs

Cells adhere to the ECM via heterodimeric integrin receptors, which are recruited to FA complexes during cell migration [35], [36]. α5β1 integrin is the principle FN binding integrin in ECs [7], [29], and has been previously described as being upregulated during developmental angiogenesis to promote EC migration and survival [37], [38]. Studies have also shown NRP1, through its cytoplasmic SEA motif, to specifically promote α5β1 integrin-mediated EC adhesion to FN matrices in a VEGF independent fashion [7], [39]. As NRP2 depletion significantly impaired mLMEC migration and adhesion on FN, and given the structural homology shared between NRP1 and NRP2, we considered whether a similar association exists between NRP2 and α5β1 integrin. First, we examined whether NRP2 knockdown regulated the expression of either integrin subunit. Western blot analysis revealed that siRNA-mediated silencing of NRP2 resulted in a significant upregulation of α5-integrin (ITGA5) subunit expression in four different EC lines (**Fig3A**), whilst β1-integrin (ITGB1) expression remained unchanged (data not shown). Whilst endothelial ITGA5 specifically pairs with ITGB1 [36], ITGB1 can form heterodimers with α subunits 1 to 9 (with the exception of α7) [40], [41], suggesting α5β1-integrin behaviour can be studied by examining ITGA5 discretely (e.g. ITGB1 expression profiles are sum measures of its interactions with multiple α subunits present in the cell). Therefore, we chose to subsequently focus our attentions on ITGA5 and its interplay with NRP2.

Studies have previously reported NRP1 to complex with ITGA5 in HUVECs [7] and NRP2 to complex with ITGA5 from co-cultures between HUVECs and renal cell carcinoma [39]. To investigate whether a direct interaction between NRP2 and ITGA5 exists in mLMECs, lysates were subjected to a series of co-immunoprecipitation studies followed by Western blot analysis. We found both NRP2 and ITGA5 co-immunoprecipitate with each other, indicating a physical interaction between the two (**Fig3B**). Immuno-staining using a highly specific NRP2 antibody, reported previously not to cross-react with NRP1 [35], [42], also showed a strong co-localisation between NRP2 and ITGA5 at the membrane (**Fig3C**). Given the significant upregulation of ITGA5 subunit expression following NRP2 depletion, and evidence to suggest a physical interaction between NRP2 and ITGA5, we next examined whether NRP2 depletion elicited an effect on ITGA5 localisation within the cell. Following treatment with either control or NRP2 siRNA, ECs were seeded overnight on a FN matrix and subsequently fixed to visualise endogenous ITGA5 expression. Compared to control siRNA treated ECs, NRP2 depleted ECs exhibited significant disruptions in ITGA5 organisation: ITGA5 appeared in elongated fibrillar structures (**Fig3D**), reminiscent of what has been described as fibrillar adhesions [28]. ImageJ™ analysis of these ITGA5 containing structures confirmed a significant increase in the length of ITGA5 fibrils in NRP2 siRNA treated ECs suggestive of a disruption in ITGA5 trafficking (**Suppl. Fig3A**). Whilst a role for NRP2 in trafficking ITGA5 is novel, NRP1 has been shown previously to promote endocytosis of active α5β1 integrin through the Rab5 pathway [7]. In order to take an unbiased approach to elucidating candidate trafficking proteins NRP2 may associate with to

bioRxiv preprint doi: https://doi.org/10.1101/744763; this version posted September 12, 2019. The copyright holder for this preprint (which was not certified by peer review) is the author/funder. All rights reserved. No reuse allowed without permission.

regulate ITGA5 localisation in ECs, we used Label-Free quantitative mass spectrometry. Mass spectrometry was performed on two WT EC lines, transfected either with control or NRP2 siRNA, and immunoprecipitated for NRP2. siRNA-mediated depletion of NRP2 was confirmed for both cell lines. This analysis revealed proteins immunoprecipitating with NRP2 at a significantly increased fold-change compared to proteins analysed from a NRP2 knockdown cell-lysate. Shown are protein hits detected in both cell lines, including both ITGA5 and ITGB1. A number of endocytic trafficking proteins were also detected as candidate binding partners of NRP2, including clathrin, caveolin-1, lamtor1, scamp1, and annexin-A1 (**Fig3E**).

ITGA5 trafficking is dependent on NRP2 in ECs

α5β1 integrin is known to be internalised both by clathrin and caveolae-mediated endocytosis [43], [44]. In order to validate a potential mechanism by which NRP2 regulates ITGA5 internalisation via its contact with clathrin and caveolin, we performed co-immunoprecipitation and co-localisation assays to prove a physical interaction. NRP2 co-immunoprecipitated with both clathrin heavy chain-1 and caveolin-1 (**Fig4A**), confirming the mass spectrometry results. We also observed a co-localisation between NRP2 and clathrin heavy chain-1 by immune-fluorescent labelling (**Suppl. Fig4A**). We subsequently conducted cell surface biotinylation assays to examine ITGA5 internalisation directly, in ECs treated either with control siRNA or NRP2 siRNA. We observed no change in the rate of ITGA5 internalisation in NRP2 depleted ECs (**Fig4B**), suggesting that NRP2 does not regulate internalisation of total ITGA5 levels. As our mass spectrometry analysis had identified candidate interactions between NRP2 and other trafficking and recycling molecules, we then performed biotin recycling assays. In these assays, the biotin-labelled cell surface proteins were allowed to internalise before stripping off any remaining surface biotin. Cells were then incubated over 20 minutes to stimulate the recycling process. NRP2 silencing significantly attenuated the rate of ITGA5 recycling back to the membrane compared to ECs treated with control siRNA (**Fig4C**).

As NRP2 depletion attenuated total ITGA5 recycling back to the membrane compared to ECs treated with control siRNA, we examined whether NRP2 shared a physical interaction with known regulators of integrin recycling in ECs. Integrin recycling back to the plasma membrane is mediated by Rab GTPase proteins [45], [46]. Specifically, α5β1 integrin follows long-loop recycling via a Rab11 dependent mechanism [47], [48]. In addition to investigating whether an interaction between NRP2 and Rab11 exists, we also considered interactions to Rab4 and Rab5, proteins both involved in regulating short-loop recycling [43]. NRP2 co-immunoprecipitated with Rab11 (**Fig4D**) and Rab4, and Rab5 (**Suppl. Fig4A**), albeit the latter two appear to be post-translationally modified in our ECs. Moreover, co-localisation between NRP2 and Rab11 (**Fig4E**), and Rab4 and Rab5 (**Suppl. Fig4B**) was also observed by immune-fluorescent labelling. NRP2 did not co-immunoprecipitate with NRP1 in any of our studies (not shown), suggesting these two structurally related proteins regulate ITGA5 trafficking through distinct pathways. We therefore present a potential mechanism whereby NRP2 promotes mLMEC migration and adhesion to FN by regulating ITGA5 trafficking, specifically via Rab11-dependent long-loop recycling back to the plasma membrane.

bioRxiv preprint doi: https://doi.org/10.1101/744763; this version posted September 12, 2019. The copyright holder for this preprint (which was not certified by peer review) is the author/funder. All rights reserved. No reuse allowed without permission.

Discussion

NRP2 is known to regulate ECM adhesion and migration in various cell lines, including human ECs [21], immune cells [49] and cancer cells [15], [20], [26], [39], [50]. In the latter, it has been described as a biomarker for poor prognosis because its expression correlates with increased migratory and invasive behaviour [15], [26], [39], [50]. In many of these examples, NRP2 contributes to cell adhesion and migration by exerting influence over VEGF-mediated pathways that, for example, lead to integrin activation that enables FA formation and downstream signalling. α5 integrin and FN are known to be upregulated in ECs during angiogenesis [37], [38], and are key players in formation of neo-vasculature [51], [52]. The data we present here support a model whereby NRP2 promotes EC adhesion and migration on FN by regulating the trafficking of α5 integrin. Importantly, the means by which it does so appears to be mechanistically distinct from that of NRP1, which is known to regulate internalisation of active α5 integrin via a rab5-dependent pathway [7].

We previously demonstrated an ITGB3-dependent role for NRP1 in mediating EC migration and FA turnover on FN [8]. EC migration on FN becomes NRP1 dependent when ITGB3 levels are perturbed [8]. Like NRP1, NRP2 expression is upregulated in ITGB3 depleted cells (**Fig1A**). Given this observation, and the structural and domain homologies between NRP1 and NRP2 [3], we sought to investigate whether NRP2 shared a similar regulatory interplay with ITGB3. We demonstrated by siRNA knockdown that EC migration depends on NRP2, but this is independent of ITGB3 expression levels (**Fig1C**).

Like NRP1 [7], [8], NRP2 also regulates a number of integrin-dependent cellular processes on FN. Upon NRP2 knockdown, actin cytoskeletal organisation is disrupted (**Fig2C**), adhesion is reduced (**Fig2D**), and FA dynamics are altered (**Fig2A-B**). Integrins provide the structural link that allows for: (1) adhesion to the ECM; (2) anchorage of actin stress fibres to the membrane; (3) the generation of force that is required for migration [47] [53], [54]. Both αvβ3- and α5β1-integrins are FN receptors in ECs [51] [52], but given the lack of any ITGB3 input into the NRP2 processes we were examining, and the upregulation of ITGA5 expression upon NRP2 depletion (**Fig3A**), we focussed our attention on this integrin subunit.

Cao et al. [39] demonstrated NRP2 to interact with ITGA5 in co-cultures between HUVECs and renal cell carcinoma to promote FN-mediated adhesion. To our knowledge, though, we are the first to show evidence of a direct interaction between NRP2 and ITGA5 in microvascular ECs (**Fig3B-C, E**). Furthermore, our findings demonstrate that NRP2 modulates ITGA5 function by regulating its subcellular trafficking. However, once again, its role in the process appears to be distinct from that of NRP1. NRP2 silencing reduces ITGA5 recycling to the plasma membrane (**Fig4C**); others have reported no changes in ITGA5 recycling in ECs upon NRP1 silencing [7].

Following internalisation by clathrin or caveolin-dependent mechanisms, α5β1 integrin has been shown to undergo long-loop recycling back to the membrane within Rab11 positive vesicles [47], [48]. Our observation that ITGA5 recycling was perturbed following depletion of NRP2 led us to examine whether an interaction exists between NRP2 and Rab11. Not only do we show co-immunoprecipitation of these two proteins (**Fig4D**), indicative of a physical association, we also show evidence of co-localisation between NRP2 and Rab11 (**Fig4E**), and between NRP2 and ITGA5, suggesting that NRP2 regulates ITGA5 recycling through a direct interaction with Rab11.

bioRxiv preprint doi: https://doi.org/10.1101/744763; this version posted September 12, 2019. The copyright holder for this preprint (which was not certified by peer review) is the author/funder. All rights reserved. No reuse allowed without permission.

We do find it interesting that, following NRP2 knock-down, surface levels of ITGA5 are maintained (**Suppl. Fig4C**), particularly given reduced long-loop recycling of the protein under these conditions. Although we did not observe any changes in internalisation of total ITGA5 upon NRP2 depletion (**Fig4B**), we were unable to examine trafficking of active α5β1 in our murine cells. In fact, we observed physical interactions between NRP2 and both clathrin and caveolin by immunoprecipitation (**Fig3E, Fig4A**) and immuno-localisation in the case of clathrin (**Suppl. Fig4A**), suggesting NRP2 has the potential to regulate the endocytosis of α5β1 integrin. In support of such a hypothesis, surface levels of ITGA5 are maintained when NRP2 is silenced. Slowed internalisation of active α5β1 might partially compensate for reduced recycling of ITGA5 to maintain a steady state level of the protein at the cell surface. However, we do not detect any interactions between NRP2 and NRP1 or GIPC1 in our NRP2 immunoprecipitation/mass spec studies (**Fig3E**). Since NRP1 is known to regulate active α5β1 integrin endocytosis via GIPC1, we would expect to anti-NRP2 to pull-down these two proteins [7]. Finally, the elevated total cellular levels of ITGA5 that occur when NRP2 is knocked-down, particularly in light of no changes at the cell surface, suggest other points in the ITGA5 life cycle are governed by NRP2. Given NRP2's interactions with clathrin and caveolin, both known to play a role in endosomal trafficking to lysosomes [43], [44], [55], we speculate a role for the molecule in regulating ITGA5 degradation. We support this hypothesis by showing NRP2 also immunoprecipitates with both Lamtor1 and Scamp1 (**Fig3E**), proteins previously shown to regulate lysosomal trafficking [56], [57].

In close, we propose a novel mechanism by which NRP2, independently of its role as a co-receptor for VEGF-A, promotes EC adhesion and migration to FN matrices by regulating Rab11-dependent recycling of ITGA5. Importantly, we provide evidence to suggest that NRP2 acts in a mechanistically distinct manner to NRP1. Finally, whilst we have not yet shown any phenotypic interactions between NRP2 and ITGB3, we cannot rule out a role for ITGB3 in regulating NRP2 trafficking. Like NRP1, NRP2 levels are significantly elevated when ITGB3 expression is reduced (**Fig1A**). Our findings allude to a complex interplay between FN-binding integrins and neuropilins which regulate EC migration.

bioRxiv preprint doi: https://doi.org/10.1101/744763; this version posted September 12, 2019. The copyright holder for this preprint (which was not certified by peer review) is the author/funder. All rights reserved. No reuse allowed without permission.

Materials and Methods

Animal Generation

All experiments were performed in accordance with UK home office regulations and the European Legal Framework for the Protection of Animals used for Scientific Purposes (European Directive 86/609/EEC), prior to the start of this project. Transgenic mice expressing a knockout for the β3-integrin allele (KO-*Itgb3*) were generated by substituting a 1.4 kb HindIII fragment of the β3 gene including exons I and II with a 1.7 kb construct containing a Pgk-neomycin (neo)-resistance cassette (**Suppl. Fig1F**). The PCR analysis was carried out using the following oligonucleotide primers as previously described by Hodivala-Dilke et al. [58].

Forward primer 1: 5'-CTTAGACACCTGCTACGGGC-3'
Reverse primer 2: 5'-CACGAGACTAGTGAGACGTG-3'

Cell Isolation, Immortalisation and Cell Culture

Primary mouse lung microvascular endothelial cells (mLMECs) were isolated from adult mice bred on a mixed C57BL6/129 background. Primary ECs were twice positively selected for through their expression of intracellular adhesion molecule-2 (ICAM-2) by magnetic activated cell sorting (MACS) as previously described by Reynolds & Hodivala-Dilke [60]. ECs were immortalised using polyoma-middle-T-antigen (PyMT) retroviral transfection as previously described by Robinson et al. [23]. Immortalised mLMECs were cultured in IMMLEC media, a 1:1 mix of Ham's F-12:DMEM medium (low glucose) supplemented with 10% FBS, 100 units/mL penicillin/streptomycin (P/S), 2 mM glutamax, 50 µg/mL heparin (Sigma).

Immortalised mLMECs were cultured on 0.1% gelatin coated flasks at 37°C in a humidified incubator with 5% CO_2. For experimental analyses, plates, dishes, flasks and coverslips were coated in 10 µg/ml human plasma fibronectin (FN) (Millipore) overnight at 4°C. Vascular endothelial growth factor-A (VEGF-A_{164}: mouse equivalent of VEGF-A_{165}) was made in-house as previously described by Krilleke et al. [61].

siRNA Transfection

ECs were transfected with non-targeting control siRNA or a mouse-specific NRP2 siRNA construct (Dharmacon), suspended in nucleofection buffer (200 mM Hepes, 137 mM NaCl, 5 mM KCl, 6 mM D-glucose, and 7 mM Na_2HPO_4 in nuclease-free water) using either the Amaxa nucleofector system II (Lonza) under nucleofection program T-005 or the Amaxa 4D-nucleofector system (Lonza) under nucleofection program EO-100 according to manufacturer's instructions.

Western Blot Analysis

siRNA transfected ECs were seeded into FN-coated 6-well plates at a seeding density of $5x10^5$ cells/well and incubated for 48 hours at 37°C in a 5% CO_2 incubator. ECs were lysed in electrophoresis sample buffer (ESB) (Tris-HCL: 65 mM pH 7.4, sucrose: 60 mM, 3% SDS), and homogenised using a Tissue Lyser (Qiagen) with acid-washed glass beads (Sigma). Following protein quantification using the DC BioRad assay, 30 µg of protein from each sample was loaded onto 8% polyacrylamide gels and subjected to SDS-PAGE. Proteins were transferred to a nitrocellulose membrane (Sigma) and incubated in 5% milk powder in PBS 0.1% Tween-20 (0.1% PBST) for 1 hour at room temperature followed by an overnight

bioRxiv preprint doi: https://doi.org/10.1101/744763; this version posted September 12, 2019. The copyright holder for this preprint (which was not certified by peer review) is the author/funder. All rights reserved. No reuse allowed without permission.

incubation in primary antibody diluted 1:1000 in 5% bovine serum albumin (BSA) in 0.1% PBST at 4°C. Membranes were washed 3x with 0.1% PBST and incubated in an appropriate horseradish peroxidase (HRP)-conjugated secondary antibody (Dako) diluted 1:2000 in 5% milk powder in 0.1% PBST for 2 hours at room temperature. Membranes were washed again 3x with 0.1% PBST before being incubated with Pierce ECL Western Blotting Substrate solution (Thermo Scientific). Chemiluminescence was detected on a ChemiDoc™ MP Imaging System darkroom (BioRad). Densitometric readings of band intensities for blots were obtained using ImageJ™.

Primary antibodies (all used at 1:1000 dilution and purchased from Cell Signalling Technology, unless noted otherwise) were: anti-NRP2 (clone D39A5), anti-ITGB3 (clone 4702S), anti-HSC70 (clone B-6, Santa Cruz Biotechnology), anti-phospho VEGFR2 (Y1175) (clone 2478), anti-VEGFR2 (clone 2479), anti-NRP1 (clone 3725S), anti-phospho ERK1/2 (clone 9101), anti-ERK1/2 (clone 4695), anti-ITGA5 (clone 4705S), anti-ITGB1 (clone ab179471, Abcam), anti-clathrin heavy chain-1 (clone ab21679, Abcam), anti-caveolin-1 (clone ab18199, Abcam), anti-Rab11 (clone 3539), anti-Rab4 (clone 610888, BD Biosciences), anti-Rab5 (clone ab18211, Abcam).

Signalling Assays

siRNA-transfected ECs were seeded into FN-coated 6 cm cultures dishes at a density of $5x10^5$ cells/well and incubated for 48 hours. ECs were then PBS washed and starved for 3 hours in serum free medium (OptiMEM®; Invitrogen). VEGF was then added at a final concentration of 30 ng/ml. After the desired time of VEGF-stimulation, ECs were subjected to lysing, protein quantification and protein expression analysis by Western blot.

Random Migration Assays

siRNA-transfected ECs were seeded into FN coated 24-well plates at a density of $7x10^4$ cells/well 24 hours post nucleofection, and allowed to adhere for 3 hours. Fixed images of multiple fields/well were taken every 10 minutes for 15 hours at 37°C and 5% CO_2 using an inverted Zeiss Axiovert microscope with one-phase contrast. Random migration was quantified by manually tracking individual cells using the ImageJ™ plugin mTrackJ. Random migration speed was calculated in µm/hour.

Focal Adhesion Turnover Assays

ECs double transfected with control or NRP2 siRNA and a GFP-tagged paxillin construct (kindly provided by Dr Maddy Parsons, Kings College, London) were seeded onto FN-coated acid-washed, oven sterilised glass coverslips in 24-well plates at a seeding density of $4x10^4$ cells/well. 48 hours post nucleofection, coverslips were PBS washed, fixed in a Ludin chamber (Life Imaging Services GmbH), and live imaged in OptiMEM® phenol-red free medium supplemented with 2% FBS and P/S at 37°C and 5% CO_2 using an inverted Axiovert (Carl Zeiss Ltd) microscope in which an individual cell was captured every one minute for 30 minutes. Focal adhesion (FA) assembly and disassembly speeds were analysed by manually tracking the number of selected GFP-paxillin-positive focal adhesions using the Image J™ MTrackJ plugin software.

Immunocytochemistry

siRNA-transfected ECs were seeded onto FN-coated acid-washed, oven sterilised glass coverslips in 24-well plates at a seeding density of $2.5x10^4$ cells/well. ECs were fixed at indicated timepoints in 4% paraformaldehyde (PFA) for 10 minutes, washed in PBS, blocked and permeabilised with 10% goat serum, PBS 0.3% triton X-100 for 1 hour at room

bioRxiv preprint doi: https://doi.org/10.1101/744763; this version posted September 12, 2019. The copyright holder for this preprint (which was not certified by peer review) is the author/funder. All rights reserved. No reuse allowed without permission.

temperature. Cells were incubated in primary antibody diluted 1:100 in PBS overnight at 4°C. Primary antibodies were: anti-paxillin (clone ab32084; Abcam), anti-ITGA5 (clone ab150361; Abcam). Coverslips were PBS washed, and incubated with donkey anti-rabbit Alexa fluor-488 secondary antibody diluted 1:200 in PBS for 2 hours at room temperature. F-actin staining was performed by incubating cells in phalloidin-364 diluted 1:40 in PBS for 2 hours at room temperature during secondary antibody incubation. Coverslips were PBS washed again, before being mounted onto slides with Prolong® Gold containing DAPI (Invitrogen). Images were captured using a Zeiss AxioImager M2 microscope (AxioCam MRm camera) at 63x magnification. FA number and size was quantified using ImageJ™ software as previously described by Lambert et al. [62]. A FA size lower detection limit was set at 0.8 microns. ITGA5 length was measured using the ImageJ™ software plugin simple neurite tracer.

Colorimetric Adhesion Assays

siRNA-transfected ECs were seeded into 96-well plates at a density of $4x10^4$ cells/well 48 hours post nucleofection. 96-well plates were pre-coated with FN overnight, then blocked in 5% BSA for 1 hour at room temperature. ECs were then incubated at 37°C in a 5% CO_2 incubator for the indicated timepoints, in addition to a 3-hour incubation control plate. Following incubation, ECs were washed 3x with PBS + 1 mM $MgCl_2$ + 1 mM $CaCl_2$, fixed in 4% PFA, and stained with methylene blue for 30 minutes at room temperature. ECs were washed in dH_2O and air-dried, before the dye from stained adhered ECs was extracted by a de-stain solution (50% ethanol, 50% 0.1M HCL). The absorbance of each well was then read at 630 nm. Data was normalised to the relative number of the total cells seeded in the 3-hour incubation plate.

Co-Immunoprecipitation Assays

siRNA-transfected ECs were seeded into FN-coated 10 cm dishes at a density of $2x10^6$ cells/dish, and incubated for 48 hours. ECs were then lysed on ice in lysis buffer as previously described by Valdembri et al. [7] in the presence of 100X Halt protease inhibitor cocktail (Thermo Scientific) and protein quantified using the DC BioRad assay. 100 µg protein from each sample was immunoprecipitated by incubation with protein-G Dynabeads® (Invitrogen) coupled to a rabbit anti-NRP2 antibody (clone 3366, Cell Signalling Technology) on a rotator overnight at 4°C. Immunoprecipitated complexes were then washed 3x with lysis buffer + 100X Halt™ protease inhibitor, and once in PBS, before being added to and boiled in NuPAGE sample reducing agent and sample buffer (Life Technologies) for Western blot analysis.

Co-localisation Assays

siRNA-transfected ECs were prepared the same as for immuno-cytochemistry. Cells were incubated in primary antibody diluted 1:50 in PBS overnight at 4°C. Primary antibodies were: anti-NRP2 (clone sc-13117, Santa Cruz Biotechnology), anti-clathrin heavy chain-1 (clone ab21679, Abcam), anti-ITGA5 (clone ab150361; Abcam), anti-Rab11 (clone 3539), anti-Rab4 (clone 610888, BD Biosciences), anti-Rab5 (clone ab18211, Abcam). Coverslips were PBS washed, and incubated with both donkey anti-rabbit Alexa fluor-488, and goat anti-mouse Alexa fluor-546 secondary antibodies diluted 1:200 in PBS for 2 hours at room temperature. Coverslips were PBS washed again, before being mounted onto slides with Prolong® Gold containing DAPI (Invitrogen). Images were captured using a Zeiss AxioImager M2 microscope (AxioCam MRm camera) at 63x magnification.

bioRxiv preprint doi: https://doi.org/10.1101/744763; this version posted September 12, 2019. The copyright holder for this preprint (which was not certified by peer review) is the author/funder. All rights reserved. No reuse allowed without permission.

Mass Spectrometry Analysis

NRP2 co-immunoprecipitation samples were sent to Fingerprints Proteomics Facility (Dundee University, UK), which carried out label-free quantitative mass spectrometry and peptide identification using the MaxQuant software based on the Andromeda peptide database as described by Schiller et al. [63]. **Fig3D** depicts peptide hits detected at a higher fold-change in two control siRNA treated EC lines than those detected from two NRP2 siRNA treated EC lines.

Internalisation and Recycling Assays

Internalisation

siRNA-transfected ECs were seeded into FN-coated 10 cm dishes at a density of $2x10^6$ cells/dish, and incubated for 48 hours. ECs were then starved in serum-free OptiMEM® for 3 hours at 37°C in a 5% CO_2 incubator, before being placed on ice for 5 minutes, then washed twice with Soerensen buffer (SBS) pH 7.8 (14.7mM KH_2PO_4, 2mM Na_2HPO_4, and 120mM Sorbitol pH 7.8) as previously described by Remacle et al. [64]. EC cell surface proteins were labelled with 0.3 mg/ml biotin (Thermo Scientific) in SBS for 30 minutes at 4°C. Unreacted biotin was quenched with 100 mM glycine for 10 minutes at 4°C. ECs were then incubated in pre-warmed serum-free OptiMEM® for the indicated time points at 37°C in a 5% CO_2 incubator. A sample of ECs were maintained at 4°C for use as positive/negative (+/- Mesna) controls. Following incubation, dishes were immediately placed on ice, washed twice with SBS pH 8.2, and incubated with 100mM Mesna (Sigma) for 75 minutes at 4°C (with the exception of Mesna control plates, which were lysed in lysis buffer (25mM Tris-HCl, pH 7.4, 100mM NaCl, 2mM $MgCl_2$, 1mM Na_3VO_4, 0.5 mM EGTA, 1% Triton X-100, 5% glycerol, and protease inhibitors), and placed on ice). Following Mesna incubation, excess Mesna was quenched with 100mM iodoacetamide (Sigma) for 10 minutes at 4°C, then ECs were washed twice with SBS pH 8.2 and lysed. Lysates were cleared by centrifugation at 12,000g for 20 minutes at 4°C. Supernatant proteins were then quantified using the DC BioRad assay, and subsequently immunoprecipitated with Dynabeads coupled to mouse anti-biotin antibody overnight at 4°C. Immunoprecipitated biotin-labelled proteins were separated by SDS-PAGE and subjected to Western bolt analysis. The level of internalised ITGA5 at each time of incubation was normalised to the (- Mesna) control.

Recycling

After surface labelling, ECs were incubated in pre-warmed serum free OptiMEM® for 20 minutes at 37°C to allow internalisation. A sample of ECs were maintained at 4°C for use as positive/negative controls. The remaining dishes were subsequently placed on ice, washed twice with SBS pH 8.2, and any un-internalised biotin-labelled proteins were stripped off using 100 mM Mesna in Tris buffer for 75 minutes at 4°C. The internalised fraction of proteins was then allowed to recycle to the membrane by incubating the ECs for the indicated time points in serum-free OptiMEM® at 37°C. Following the indicated times of incubation, dishes were placed on ice, washed twice with SBS pH 8.2, and subjected to Mesna incubation for 75 minutes at 4°C. No Mesna treatment dishes at each timepoint were used as controls. All subsequent stages were performed in the same manner as the internalisation assay. The level of the recycled ITGA5 was determined by normalising the amount of ITGA5 quantified from dishes treated with Mesna, to the total ITGA5 on the membranes of the Mesna-untreated cells in the same period of incubation.

bioRxiv preprint doi: https://doi.org/10.1101/744763; this version posted September 12, 2019. The copyright holder for this preprint (which was not certified by peer review) is the author/funder. All rights reserved. No reuse allowed without permission.

Statistical Analysis

The graphic illustrations and analyses to determine statistical significance were generated using GraphPad Prism 6 software and Student's t-tests, respectively. Bar charts show mean values and the standard error of the mean (±SEM). Asterisks indicate the statistical significance of P values: $P > 0.05$ = ns (not significant), * $P < 0.05$, ** $P < 0.01$, *** $P < 0.001$ and **** $P < 0.0001$.

Acknowledgments

This work was supported by funding from: the UKRI Biotechnology and Biological Sciences Research Council Norwich Research Park Biosciences Doctoral Training Partnership (Grant numbers BB/M011216/1, BB/J014524/1); BHF (grant number PG/15/25/31369); The Ministry of Education, Saudi Arabia. Additionally, we thank Norfolk Fundraisers, Mrs Margaret Doggett, and the Colin Wright Fund for their kind support and fundraising over the years.

Contributions

	AAAA	CJB	SJA	JL	SDR
Conceptualisation					
Formal Analysis					
Investigation					
Resources					
Review and Editing					
Visualisation					
Supervision					
Funding Acquisition					

Competing Interests

The authors declare no competing interests.

bioRxiv preprint doi: https://doi.org/10.1101/744763; this version posted September 12, 2019. The copyright holder for this preprint (which was not certified by peer review) is the author/funder. All rights reserved. No reuse allowed without permission.

References

1. Soker, S., et al., *Neuropilin-1 is expressed by endothelial and tumor cells as an isoform-specific receptor for vascular endothelial growth factor.* Cell, 1998. **92**(6): p. 735-745.
2. Pellet-Many, C., et al., *Neuropilins: structure, function and role in disease.* Biochemical Journal, 2008. **411**(2): p. 211-226.
3. Zachary, I., *Neuropilins: role in signalling, angiogenesis and disease*, in *Angiogenesis, Lymphangiogenesis and Clinical Implications*. 2014, Karger Publishers. p. 37-70.
4. Bielenberg, D.R., et al., *Semaphorin 3F, a chemorepulsant for endothelial cells, induces a poorly vascularized, encapsulated, nonmetastatic tumor phenotype.* The Journal of clinical investigation, 2004. **114**(9): p. 1260-1271.
5. Prahst, C., et al., *Neuropilin-1-VEGFR2 complexing requires the PDZ-binding domain of neuropilin-1.* Journal of biological chemistry, 2008. **283**(37): p. 25110-25114.
6. Fukasawa, M., A. Matsushita, and M. Korc, *Neuropilin-1 interacts with integrin β1 and modulates pancreatic cancer cell growth, survival and invasion.* Cancer biology & therapy, 2007. **6**(8): p. 1184-1191.
7. Valdembri, D., et al., *Neuropilin-1/GIPC1 signaling regulates α5β1 integrin traffic and function in endothelial cells.* PLoS Biol, 2009. **7**(1): p. e1000025.
8. Ellison, T.S., et al., *Suppression of β3-integrin in mice triggers a neuropilin-1-dependent change in focal adhesion remodelling that can be targeted to block pathological angiogenesis.* Disease models & mechanisms, 2015. **8**(9): p. 1105-1119.
9. Herzog, Y., et al., *Differential expression of neuropilin-1 and neuropilin-2 in arteries and veins.* Mechanisms of development, 2001. **109**(1): p. 115-119.
10. Yuan, L., et al., *Abnormal lymphatic vessel development in neuropilin 2 mutant mice.* Development, 2002. **129**(20): p. 4797-4806.
11. Jurisic, G., et al., *An unexpected role of semaphorin3A–neuropilin-1 signaling in lymphatic vessel maturation and valve formation.* Circulation research, 2012. **111**(4): p. 426-436.
12. Bouvrée, K., et al., *Semaphorin3A, Neuropilin-1, and PlexinA1 are required for lymphatic valve formation.* Circulation research, 2012. **111**(4): p. 437-445.
13. Mucka, P., et al., *Inflammation and lymphedema are exacerbated and prolonged by neuropilin 2 deficiency.* The American journal of pathology, 2016. **186**(11): p. 2803-2812.
14. Fakhari, M., et al., *Selective upregulation of vascular endothelial growth factor receptors neuropilin-1 and-2 in human neuroblastoma.* Cancer, 2002. **94**(1): p. 258-263.
15. Kawakami, T., et al., *Neuropilin 1 and neuropilin 2 co-expression is significantly correlated with increased vascularity and poor prognosis in nonsmall cell lung carcinoma.* Cancer: Interdisciplinary International Journal of the American Cancer Society, 2002. **95**(10): p. 2196-2201.
16. Tomizawa, Y., et al., *Inhibition of lung cancer cell growth and induction of apoptosis after reexpression of 3p21. 3 candidate tumor suppressor gene SEMA3B.* Proceedings of the National Academy of Sciences, 2001. **98**(24): p. 13954-13959.
17. Lantuéjoul, S., et al., *Expression of VEGF, semaphorin SEMA3F, and their common receptors neuropilins NP1 and NP2 in preinvasive bronchial lesions, lung tumours, and cell lines.* The Journal of Pathology: A Journal of the Pathological Society of Great Britain and Ireland, 2003. **200**(3): p. 336-347.

bioRxiv preprint doi: https://doi.org/10.1101/744763; this version posted September 12, 2019. The copyright holder for this preprint (which was not certified by peer review) is the author/funder. All rights reserved. No reuse allowed without permission.

18. Vales, A., et al., *Myeloid leukemias express a broad spectrum of VEGF receptors including neuropilin-1 (NRP1) and NRP2.* Leukemia & lymphoma, 2007. **48**(10): p. 1997-2007.
19. Bachelder, R.E., et al., *Vascular endothelial growth factor is an autocrine survival factor for neuropilin-expressing breast carcinoma cells.* Cancer research, 2001. **61**(15): p. 5736-5740.
20. Fukahi, K., et al., *Aberrant expression of neuropilin-1 and-2 in human pancreatic cancer cells.* Clinical Cancer Research, 2004. **10**(2): p. 581-590.
21. Favier, B., et al., *Neuropilin-2 interacts with VEGFR2 and VEGFR-3 and promotes human endothelial cell survival and migration.* Blood, 2006. **108**(4): p. 1243-1250.
22. Robinson, S.D., et al., *β3-Integrin Regulates Vascular Endothelial Growth Factor-A–Dependent Permeability.* Arteriosclerosis, Thrombosis, and Vascular Biology, 2004. **24**(11): p. 2108-2114.
23. Robinson, S.D., et al., *Alphavbeta3-integrin limits the contribution of neuropilin-1 to VEGF-induced angiogenesis.* Journal of Biological Chemistry, 2009: p. jbc. M109. 030700.
24. Sivarapatna, A., et al., *Arterial specification of endothelial cells derived from human induced pluripotent stem cells in a biomimetic flow bioreactor.* Biomaterials, 2015. **53**: p. 621-633.
25. Ikuno, T., et al., *Efficient and robust differentiation of endothelial cells from human induced pluripotent stem cells via lineage control with VEGF and cyclic AMP.* PloS one, 2017. **12**(3): p. e0173271.
26. Caunt, M., et al., *Blocking neuropilin-2 function inhibits tumor cell metastasis.* Cancer cell, 2008. **13**(4): p. 331-342.
27. Small, J.V., et al., *Assembling an actin cytoskeleton for cell attachment and movement.* Biochimica Et Biophysica Acta (BBA)-Molecular Cell Research, 1998. **1404**(3): p. 271-281.
28. Webb, D.J., J.T. Parsons, and A.F. Horwitz, *Adhesion assembly, disassembly and turnover in migrating cells–over and over and over again.* Nature cell biology, 2002. **4**(4): p. E97-E100.
29. Valdembri, D. and G. Serini, *Regulation of adhesion site dynamics by integrin traffic.* Current opinion in cell biology, 2012. **24**(5): p. 582-591.
30. De Pascalis, C. and S. Etienne-Manneville, *Single and collective cell migration: the mechanics of adhesions.* Molecular biology of the cell, 2017. **28**(14): p. 1833-1846.
31. Ridley, A.J., et al., *Cell migration: integrating signals from front to back.* Science, 2003. **302**(5651): p. 1704-1709.
32. Atkinson, S.J., et al., *The β3-integrin endothelial adhesome regulates microtubule-dependent cell migration.* EMBO reports, 2018: p. e44578.
33. Schiller, H.B., et al., *β 1-and α v-class integrins cooperate to regulate myosin II during rigidity sensing of fibronectin-based microenvironments.* Nature cell biology, 2013. **15**(6): p. 625.
34. Fantin, A., et al., *NRP1 regulates CDC42 activation to promote filopodia formation in endothelial tip cells.* Cell reports, 2015. **11**(10): p. 1577-1590.
35. Goel, H.L., et al., *Neuropilin-2 regulates α6β1 integrin in the formation of focal adhesions and signaling.* J Cell Sci, 2012. **125**(2): p. 497-506.
36. Avraamides, C.J., B. Garmy-Susini, and J.A. Varner, *Integrins in angiogenesis and lymphangiogenesis.* Nature Reviews Cancer, 2008. **8**(8): p. 604.
37. Goodman, S.L. and M. Picard, *Integrins as therapeutic targets.* Trends in pharmacological sciences, 2012. **33**(7): p. 405-412.

bioRxiv preprint doi: https://doi.org/10.1101/744763; this version posted September 12, 2019. The copyright holder for this preprint (which was not certified by peer review) is the author/funder. All rights reserved. No reuse allowed without permission.

38. Kim, S., et al., *Inhibition of endothelial cell survival and angiogenesis by protein kinase A.* The Journal of clinical investigation, 2002. **110**(7): p. 933-941.
39. Cao, Y., et al., *Neuropilin-2 promotes extravasation and metastasis by interacting with endothelial α5 integrin.* Cancer research, 2013. **73**(14): p. 4579-4590.
40. Velling, T., et al., *Distinct α7Aβ1 and α7Bβ1 integrin expression patterns during mouse development: α7A is restricted to skeletal muscle but α7B is expressed in striated muscle, vasculature, and nervous system.* Developmental dynamics, 1996. **207**(4): p. 355-371.
41. Hynes, R.O., *Integrins: bidirectional, allosteric signaling machines.* Cell, 2002. **110**(6): p. 673-687.
42. Bae, D., et al., *Metabolic stress induces the lysosomal degradation of neuropilin-1 but not neuropilin-2.* Journal of Biological Chemistry, 2008. **283**(42): p. 28074-28080.
43. Margadant, C., et al., *Mechanisms of integrin activation and trafficking.* Current opinion in cell biology, 2011. **23**(5): p. 607-614.
44. Shi, F. and J. Sottile, *Caveolin-1-dependent β1 integrin endocytosis is a critical regulator of fibronectin turnover.* Journal of cell science, 2008. **121**(14): p. 2360-2371.
45. Paul, N.R., G. Jacquemet, and P.T. Caswell, *Endocytic trafficking of integrins in cell migration.* Current Biology, 2015. **25**(22): p. R1092-R1105.
46. Roberts, M., et al., *PDGF-regulated rab4-dependent recycling of αvβ3 integrin from early endosomes is necessary for cell adhesion and spreading.* Current Biology, 2001. **11**(18): p. 1392-1402.
47. Laukaitis, C.M., et al., *Differential dynamics of α5 integrin, paxillin, and α-actinin during formation and disassembly of adhesions in migrating cells.* The Journal of cell biology, 2001. **153**(7): p. 1427-1440.
48. Caswell, P.T., et al., *Rab25 associates with α5β1 integrin to promote invasive migration in 3D microenvironments.* Developmental cell, 2007. **13**(4): p. 496-510.
49. Curreli, S., et al., *Polysialylated neuropilin-2 is expressed on the surface of human dendritic cells and modulates dendritic cell-T lymphocyte interactions*. JBC, 2007. **282**: p. 30346-30356.
50. Dallas, N.A., et al., *Neuropilin-2–mediated tumor growth and angiogenesis in pancreatic adenocarcinoma.* Clinical Cancer Research, 2008. **14**(24): p. 8052-8060.
51. Brooks, P., C., et al. *Requirement of vascular integrin alpha v beta 3 for angiogenesis.* Science, 1994. **264:** 569–571 5.
52. Kim, S., et al., *Regulation of angiogenesis in vivo by ligation of integrin alpha5beta1 with the central cell-binding domain of fibronectin*. Am J Pathol, 2000. **156:** 1345–1362.
53. Buskermolen, A.B., N.A. Kurniawan, and C.V. Bouten, *An automated quantitative analysis of cell, nucleus and focal adhesion morphology.* PloS one, 2018. **13**(3): p. e0195201.
54. Le Boeuf, F., F. Houle, and J. Huot, *Regulation of vascular endothelial growth factor receptor 2-mediated phosphorylation of focal adhesion kinase by heat shock protein 90 and Src kinase activities.* Journal of Biological Chemistry, 2004. **279**(37): p. 39175-39185.
55. Sachse, M., et al., *Bilayed clathrin coats on endosomal vacuoles are involved in protein sorting toward lysosomes*. Molecular Biology of the Cell, 2002. **13**: 1313-1328.
56. Malek, M., et al., *LAMTOR1 depletion induces p53-dependent apoptosis via aberrant lysosomal activation.* Cell death & disease, 2012. **3**(4): e300.

bioRxiv preprint doi: https://doi.org/10.1101/744763; this version posted September 12, 2019. The copyright holder for this preprint (which was not certified by peer review) is the author/funder. All rights reserved. No reuse allowed without permission.

57. Cai, Y., et al., *Multiple cytosolic and transmembrane determinants are required for the trafficking of SCAMP1 via an ER–Golgi–TGN–PM pathway*. The Plant Journal, 2011. **65**(6): 882-896.

58. Hodivala-Dilke, K.M., et al., *β3-integrin–deficient mice are a model for Glanzmann thrombasthenia showing placental defects and reduced survival.* The Journal of clinical investigation, 1999. **103**(2): p. 229-238.
59. Claxton, S., et al., *Efficient, inducible Cre-recombinase activation in vascular endothelium.* Genesis, 2008. **46**(2): p. 74-80.
60. Reynolds, L.E. and K.M. Hodivala-Dilke, *Primary mouse endothelial cell culture for assays of angiogenesis*, in *Breast Cancer Research Protocols*. 2006, Springer. p. 503-509.
61. Krilleke, D., et al., *Molecular mapping and functional characterization of the VEGF164 heparin-binding domain.* Journal of Biological Chemistry, 2007. **282**(38): p. 28045-28056.
62. Lambert, J., et al., *ADAMTS-1 and Syndecan-4 intersect in the regulation of cell migration and angiogenesis.* bioRxiv, 2019: p. 686733.
63. Schiller, H.B., et al., *Quantitative proteomics of the integrin adhesome show a myosin II-dependent recruitment of LIM domain proteins.* EMBO reports, 2011. **12**(3): p. 259-266.
64. Remacle, A., G. Murphy, and C. Roghi, *Membrane type I-matrix metalloproteinase (MT1-MMP) is internalised by two different pathways and is recycled to the cell surface.* J Cell Sci, 2003. **116**(19): p. 3905-3916.

bioRxiv preprint doi: https://doi.org/10.1101/744763; this version posted September 12, 2019. The copyright holder for this preprint (which was not certified by peer review) is the author/funder. All rights reserved. No reuse allowed without permission.

Figure Legends

Figure 1. NRP2's role in VEGFR2 signalling and migration is not ITGB3 dependent. (**A**) WT and β3HET ECs were plated onto FN and incubated for 48 hours. EC extracts were immunoblotted using antibodies to NRP2, ITGB3 and HSC70. Western blot is representative of 3 independent experiments, ****P < 0.0001. (**B**) siRNA transfected ECs were plated onto FN and incubated for 48 hours. ECs were subsequently starved in serum-free media and stimulated with VEGF (30 ng/ml) for the indicated amounts of time. EC extracts were immunoblotted using antibodies to phosphorylated VEGFR2 (pVEGFR2), VEGFR2, NRP2, NRP1, HSC70, phosphorylated ERK (pERK) and ERK. ***Left panel*** shows representative Western blot images; ***right panel*** shows densitometric analysis of relative pVEGFR2 and pERK band intensities normalised against their respective total levels (fold stimulation is shown relative to unstimulated levels for each condition). N=4-5 independent experiments, each performed with a different EC line. ns = not significant. (**C**) siRNA transfected ECs were seeded onto FN and incubated for 3 hours. Images were taken every 10 minutes for 15 hours at 37°C and 5% CO_2 using an inverted Zeiss Axiovert microscope with one-phase contrast. Random migration speed was quantified in µm/hour. N= 4 independent experiments, n≥30 ECs per condition, ****P < 0.0001.

Figure 2. Depletion of NRP2 in ECs disrupts focal adhesion turnover and adhesion to FN. (**A**) siRNA treated ECs were transfected with a GFP-tagged paxillin construct, seeded onto FN-coated coverslips and incubated for 48 hours. ECs were fixed in a Ludin chamber and imaged live at 37°C and 5% CO_2 using an inverted Axiovert microscope in which an individual cell was captured every one minute for 30 minutes. Focal adhesion (FA) assembly and disassembly speeds were analysed using the ImageJ™ plugin mTrackJ in µm/min. n≥100 FAs per condition, ** P < 0.01. (**B**) siRNA transfected ECs were seeded onto FN and incubated for 90 minutes before being fixed in 4% PFA and stained for paxillin (PXN). FA number and size was quantified using ImageJ™. The ***left panel*** shows representative images for fixed ECs transfected either with control or NRP2 siRNA. Image quantification for FA number and size is shown in the ***right panels***; quantification performed on data from n ≥25 ECs per condition over 3 independent experiments. (**C**) siRNA transfected ECs were seeded onto FN and incubated for either 90 or 180 minutes before being fixed in 4% PFA. ECs were then labelled with Alexa-fluor-555 conjugated phalloidin to demarcate F-actin. (**D**) siRNA transfected ECs were seeded onto FN coated 96-well plates and incubated for either 15 or 30 minutes. After vigorous washing, ECs were fixed in 4% PFA and stained with methylene blue. Dye was extracted and absorbance measured at 630 nm. Data was normalised to the relative number of total cells seeded in a 3-hour incubation control plate. n= 24 wells per condition from 3 independent experiments, ** P<0.01, *** P<0.001.

Figure 3. NRP2 regulates ITGA5 expression and localisation in ECs. (**A**) siRNA transfected ECs were seeded onto FN and incubated for 48 hours. EC extracts were immunoblotted using antibodies to ITGA5, NRP2 and HSC70. ***Left panel*** shows Western blot image, ***right panel*** shows densitometric analysis of ITGA5 band intensities normalised against HSC70. N=4 independent EC lines, ** P<0.01. (**B**) siRNA transfected ECs were seeded onto FN and incubated for 48 hours. EC extracts were immunoprecipitated with: ***left panel*** anti NRP2 and Western blotted for ITGA5; or ***middle panel*** anti ITGA5 and Western blotted for NRP2. In both cases NRP2 siRNA treated lysates were included as a control for specificity. The ***right panel*** is a Western blot of total cell lysates, performed to measure the level of NRP2 silencing in the extracts used for immunoprecipitation; blots were probed for HSC70 as a loading control. **C**) siRNA-transfected ECs were seeded onto FN-coated coverslips and incubated 90 minutes before being fixed in 4% PFA. Fixed ECs were immune-labelled for NRP2 (red) and ITGA5 (green). Arrows indicate co-localisation between the two molecules. Images are representative

bioRxiv preprint doi: https://doi.org/10.1101/744763; this version posted September 12, 2019. The copyright holder for this preprint (which was not certified by peer review) is the author/funder. All rights reserved. No reuse allowed without permission.

of n>10 cells per condition. (**D**) siRNA transfected ECs were prepared as described above, but were allowed to adhere overnight prior to fixation. ECs were then immune-labelled for ITGA5. (**E**) Label-free quantitative mass spectrometry peptide hits identified using MaxQuant software from the Andromeda peptide database. Graph depicts peptide hits detected at a higher fold-change in two independent control siRNA treated EC lines compared to those detected from two independent NRP2 siRNA treated EC lines. Highlighted are interactions with: ITGA5 and ITGB1 (red); known EC markers (blue); and proteins known to play a role in protein trafficking (black). ***Inset*** NRP2 silencing was confirmed by subjecting EC extracts to Western blot analysis.

Figure 4. ITGA5 trafficking is dependent on NRP2 in ECs. (**A**) siRNA transfected ECs were seeded onto FN and incubated for 48 hours. EC extracts were immunoprecipitated for NRP2 and immunoblotted for clathrin heavy chain-1 (***left panel***), and caveolin-1 (***right panel***). Images are representative of 3 independent experiments. (**B**) siRNA transfected ECs were seeded onto FN and incubated for 48 hours. ECs were subsequently starved in serum-free media, before being placed on ice. EC cell surface proteins were labelled with 0.3 mg/ml biotin. ECs were then incubated for the indicated timepoints at 37°C. A sample of ECs were maintained at 4°C for use as positive/negative (+/- Mesna) controls. Following incubation at 37°C, ECs were placed on ice and incubated with 100 mM Mesna. EC lysates were then immunoprecipitated with an anti-biotin antibody and then immune-blotted for ITGA5. The level of internalised ITGA5 at each time of incubation was normalised to the (- Mesna) control. ***Left panel*** shows representative Western blot image; ***right panel*** shows the mean densitometric analysis from 2 independent experiments. (**C**) siRNA-transfected ECs were prepared as described in **B**. After biotin surface labelling, ECs were incubated in serum free media for 20 minutes at 37°C to allow for internalisation. A sample of ECs were maintained at 4°C for use as positive/negative controls. The remaining ECs were then placed on ice, and any un-internalised biotin-labelled proteins stripped off using 100 mM Mesna. The internalised protein fraction was allowed to recycle by incubating the ECs for the indicated timepoints at 37°C. ECs were then returned to ice and incubated in 100 mM Mesna. No Mesna treatment dishes at each timepoint were used as controls. All subsequent stages were performed in the same manner as described in **B**. The level of the recycled ITGA5 was determined by normalising the amount of ITGA5 quantified from dishes treated with Mesna, to the total ITGA5 on the membranes of the Mesna-untreated cells in the same period of incubation. ***Top panel*** shows representative Western blot image; ***bottom panel*** shows the mean densitometric analysis from 2 independent experiments. (**D**) NRP2 co-immunoprecipitation was performed as described in **A**. Immunoprecipitated complexes were subjected to Western blot analysis using an antibody against Rab11. (**E**) Fixed ECs were immuno-labelled for NRP-2 and Rab11. Arrows indicate co-localisation between to two molecules.

bioRxiv preprint doi: https://doi.org/10.1101/744763; this version posted September 12, 2019. The copyright holder for this preprint (which was not certified by peer review) is the author/funder. All rights reserved. No reuse allowed without permission.

Supplementary Material

Suppl. Fig1. (**A**) PyMT transfected mLMEC pellets from 9 different immortalised EC lines were subjected to DNA extraction and PCR-based genotyping. The ***left panel*** is a schematic diagram of the ITGB3 (WT) and (HET) loci, showing where PCR genotyping primers align. P1 and P3 amplify a wild-type product of 446-bp, whilst P1 and P2 amplify a knockout product of 538-bp. The ***right panel*** shows an agarose gel of P1/P3 and P1/P2 primer products from all EC lines. Lanes 1-5 show only a P1/P3 product and are therefore wild-type (WT) for the ITGB3 locus, whilst lines 6-9 show both a P1/P3 product, and a P1/P2 product, and are therefore heterozygous (β3HET) for the ITGB3 locus. (**B**) Western blot analysis of VE-Cadherin and ITGB3 expression in the same clones shown in **A**. HSC70 was used as a loading control. Because the antibody used for detection of ITGB3 recognises a non-specific band at approximately (135kDa), a β3-knockout (NULL) lysate was included as a control. (**C**) Graph shows the densitometric analysis of mean ITGB3 band intensities normalised against HSC70. ** $P<0.01$ (**D**) ECs were transfected either with control siRNA or one of four different NRP2-specific siRNAs (01 - 04) and incubated for 48 hours. EC extracts were then subjected to Western blot analysis using antibodies against NRP2, NRP1 and HSC70. NRP2 siRNA #03 was used for all subsequent experiments to silence NRP2 expression. (**E**) siRNA transfected ECs were incubated for the indicated timepoints before being lysed and subjected to Western blot analysis using antibodies against NRP2 and HSC70.

Suppl. Fig2. (**A**) siRNA-transfected ECs were seeded onto FN and incubated for 30 hours. ECs were then re-seeded onto FN-coated coverslips and allowed to adhere for 4 hours in serum-free media. Media was then replaced with 10 µM BrdU in complete culture medium, and the cells incubated for 12 hours at 37°C. ECs were then fixed with 4% PFA, before hydrolysing the DNA with 1M HCL. ECs were then immuno-labelled for BrdU. The number of proliferating cells was determined by dividing the number of the BrdU-labelled cells by the number of DAPI-labelled cells. n=19 fields of view per condition, containing on average 50 cells per field. (**B**) Accompanying analysis to **Fig2C**. The cell area (μm^2) was measured using ImageJ™. Quantification performed on mean data from n≥25 ECs over 3 independent experiments. ns=not significant.

Suppl.Fig3. (**A**) Accompanying analysis to **Fig3D**. ITGA5 adhesion length was measured using the ImageJ™ software plugin simple neurite tracer. n≥490 adhesion per condition, ****$P < 0.0001$.

Suppl. Fig4. (**A**): Fixed ECs were immuno-labelled for NRP2 and clathrin heavy chain-1. (**B**) ***Left panels***: NRP2 co-immunoprecipitation was performed as described in **Fig4A**. Immunoprecipitated complexes were subjected to Western blot analysis using an antibody against Rab4 and Rab5 respectively. ***Right panels***: Fixed ECs were immuno-labelled for NRP2 and Rab4 and Rab5, respectively. Arrows indicate co-localisation between the molecules. (**C**) siRNA transfected ECs were seeded onto FN and incubated for 48 hours. ECs were then detached using sodium saline buffer and resuspended in FACS buffer (1% FBS in PBS + 1mM $CaCl_2$ + 1mM $MgCl_2$). $1x10^5$ ECs from each siRNA-treated condition were incubated with antibody, labelled with ITGA5 PE-conjugated antibody or labelled with isotype control PE-conjugated antibody. Following two washes with FACS buffer to remove the unbound conjugated antibodies, the cells were subjected to flow cytometry to measure ITGA5 expression on the plasma membrane. The histogram was generated using FlowJo™ software to analyse the expression on ITGA5 in NRP2 depleted ECs compared to the Ctrl-siRNA transfected ECs. Representative of 2 independent experiment.

FIGURE 1

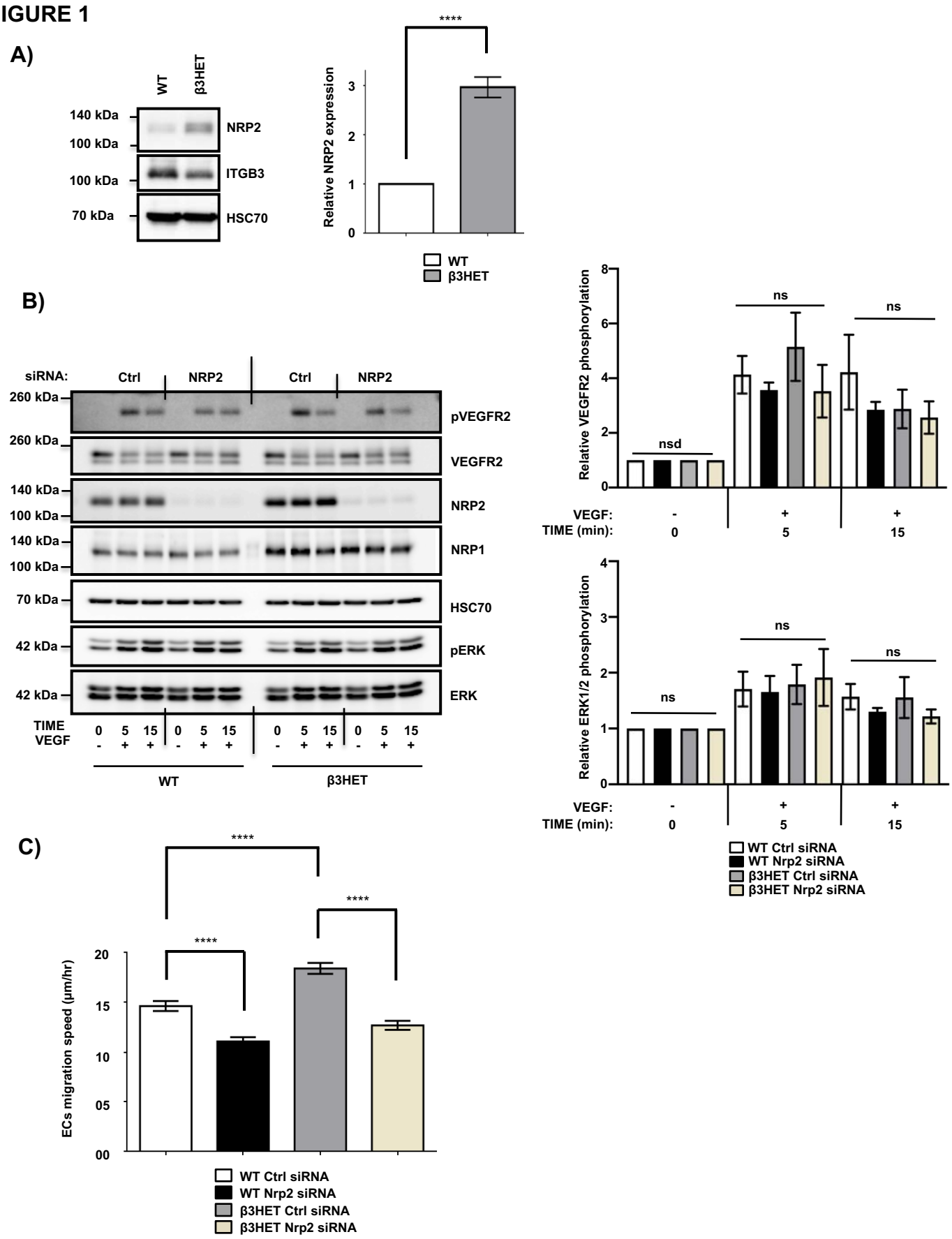
A)
WT
β3HET
140 kDa
100 kDa
NRP2
100 kDa
ITGB3
70 kDa
HSC70
****
Relative NRP2 expression
0
1
2
3
WT
β3HET
B)
siRNA:
Ctrl
NRP2
Ctrl
NRP2
260 kDa
pVEGFR2
260 kDa
VEGFR2
140 kDa
100 kDa
NRP2
140 kDa
100 kDa
NRP1
70 kDa
HSC70
42 kDa
pERK
42 kDa
ERK
TIME
VEGF
0 5 15 0 5 15 0 5 15 0 5 15
- + + - + + - + + - + +
WT
β3HET
Relative VEGFR2 phosphorylation
nsd
ns
ns
VEGF:
TIME (min):
0
5
15
Relative ERK1/2 phosphorylation
ns
ns
ns
WT Ctrl siRNA
WT Nrp2 siRNA
β3HET Ctrl siRNA
β3HET Nrp2 siRNA
C)
****
****
****
ECs migration speed (µm/hr)
00
05
10
15
20
WT Ctrl siRNA
WT Nrp2 siRNA
β3HET Ctrl siRNA
β3HET Nrp2 siRNA

FIGURE 2

A)

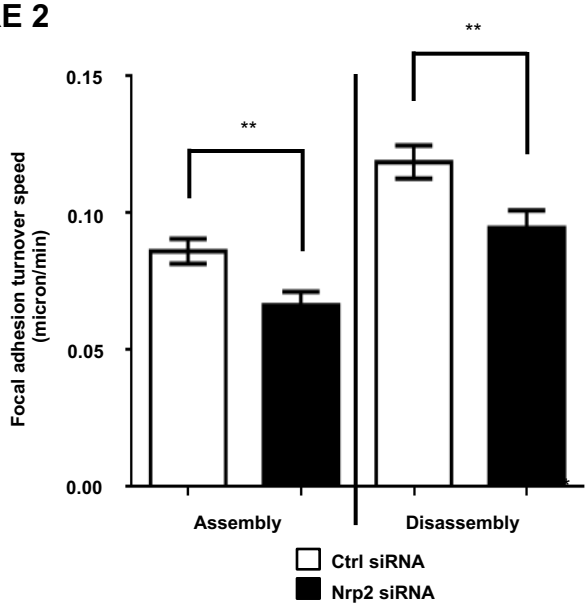

B)

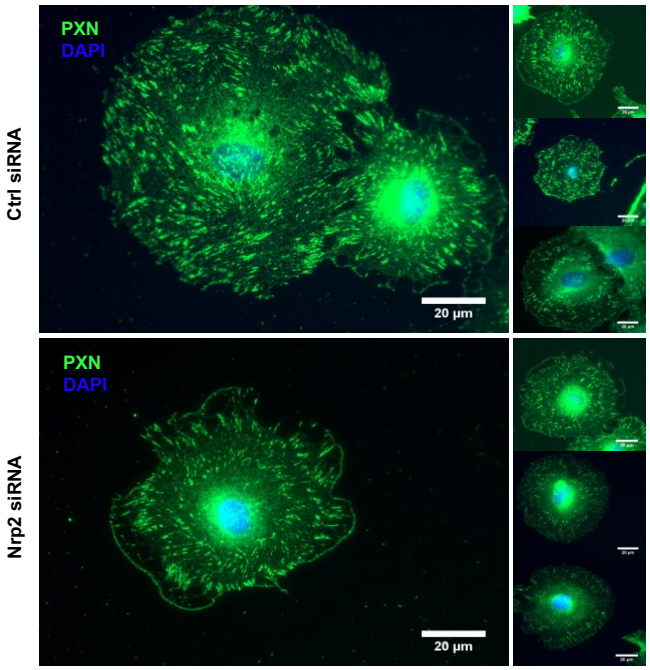

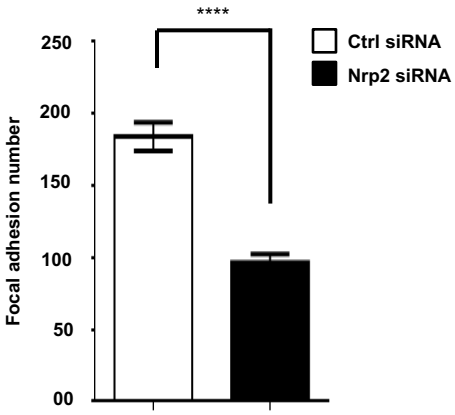

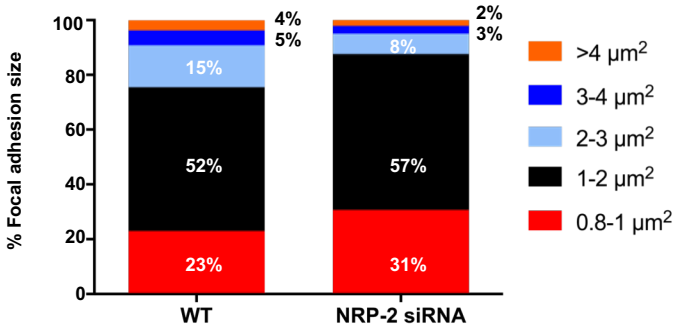

C)

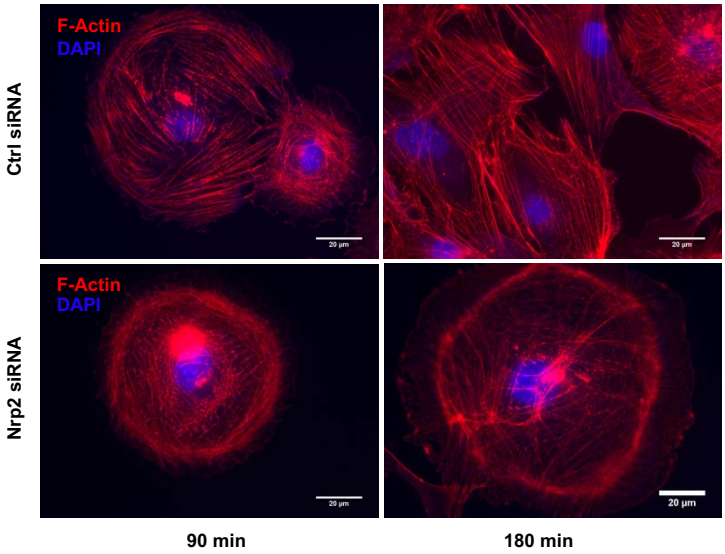

D)

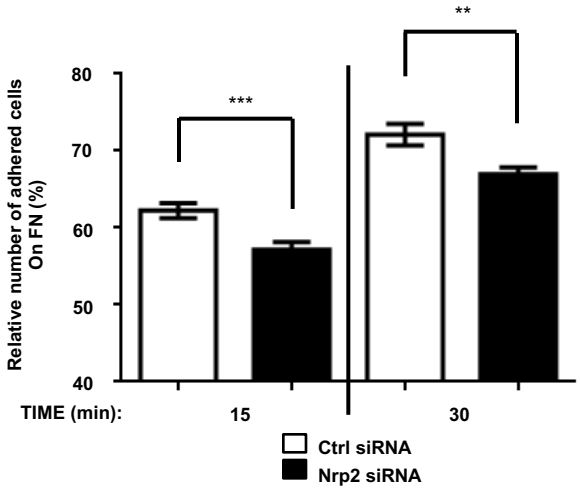

FIGURE 3

A)

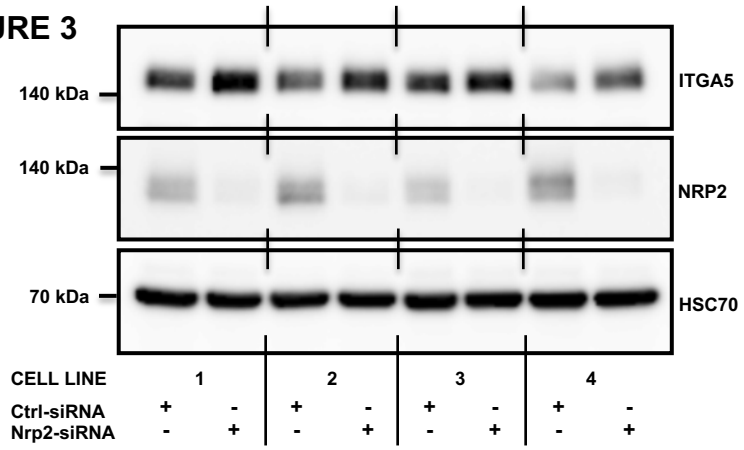

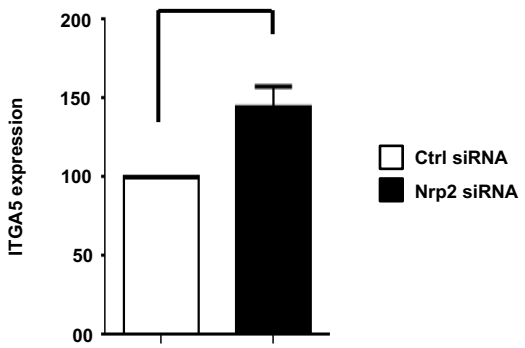

B)

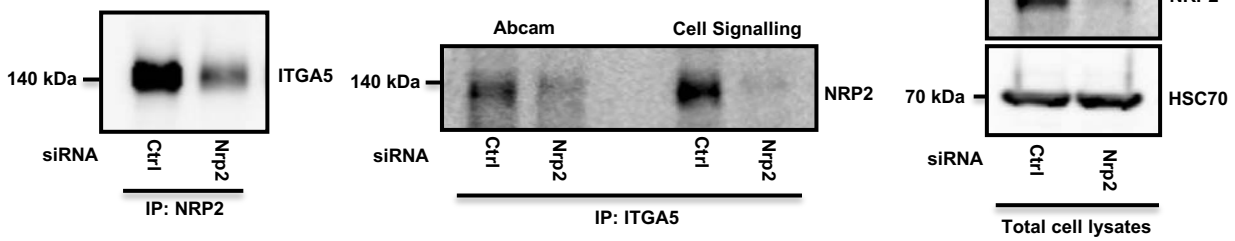

C)

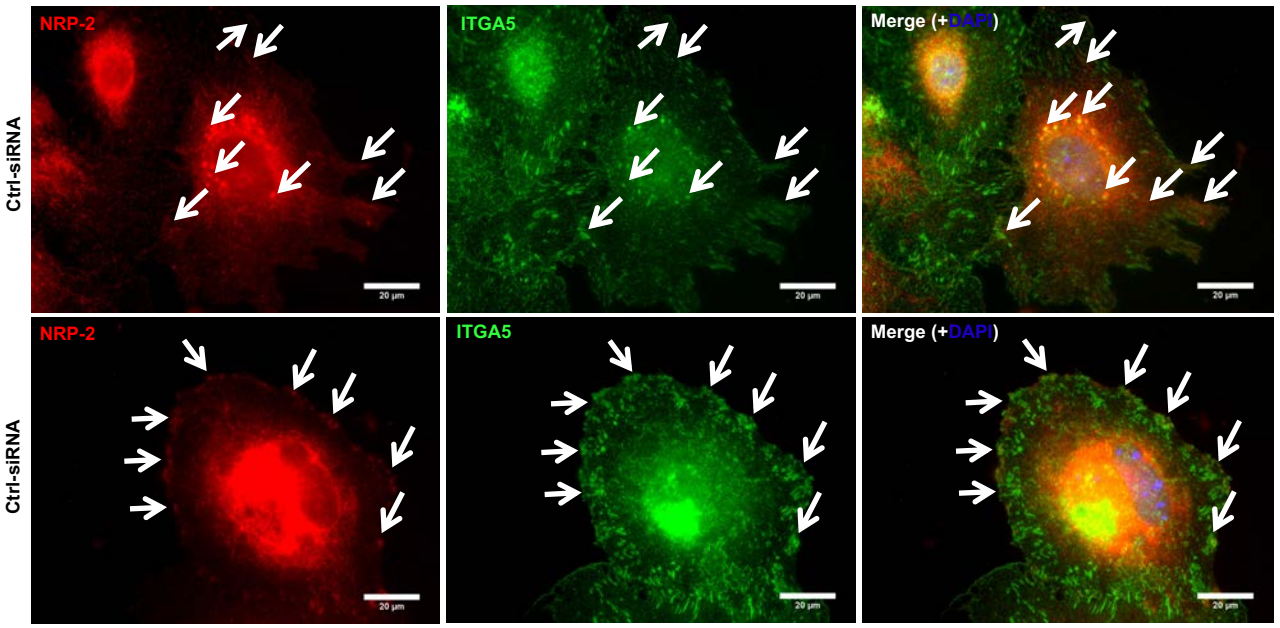

D)

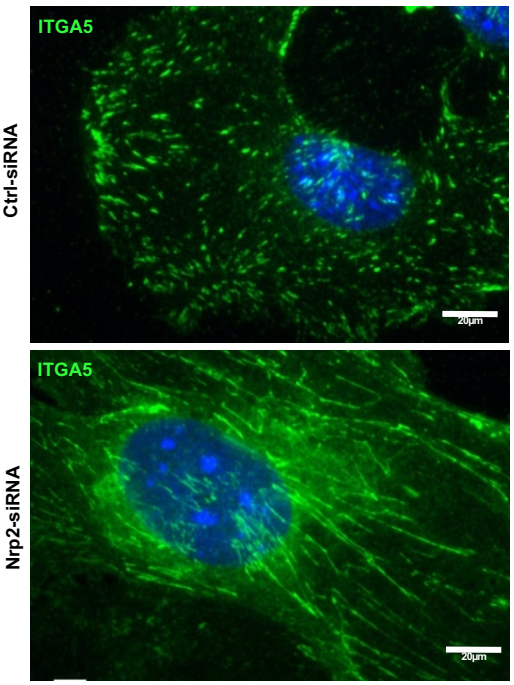

E)

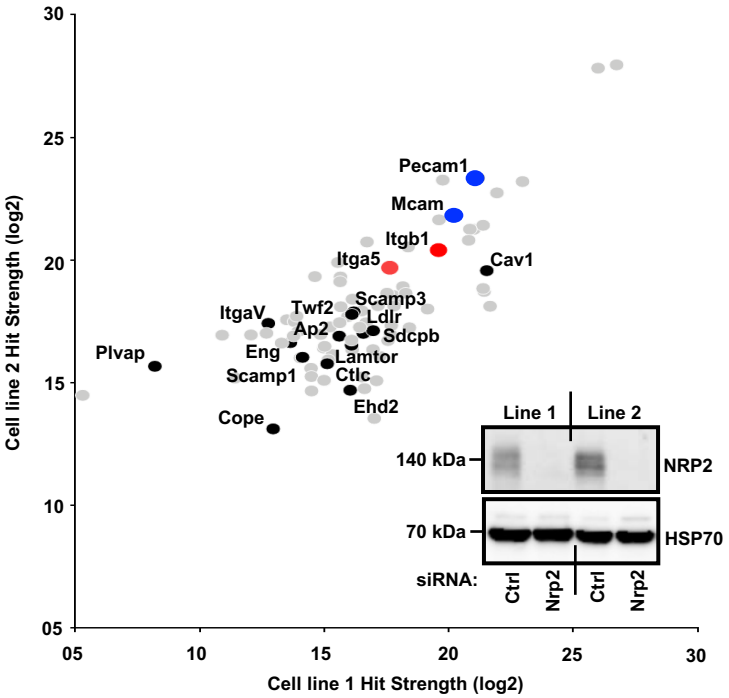

FIGURE 4

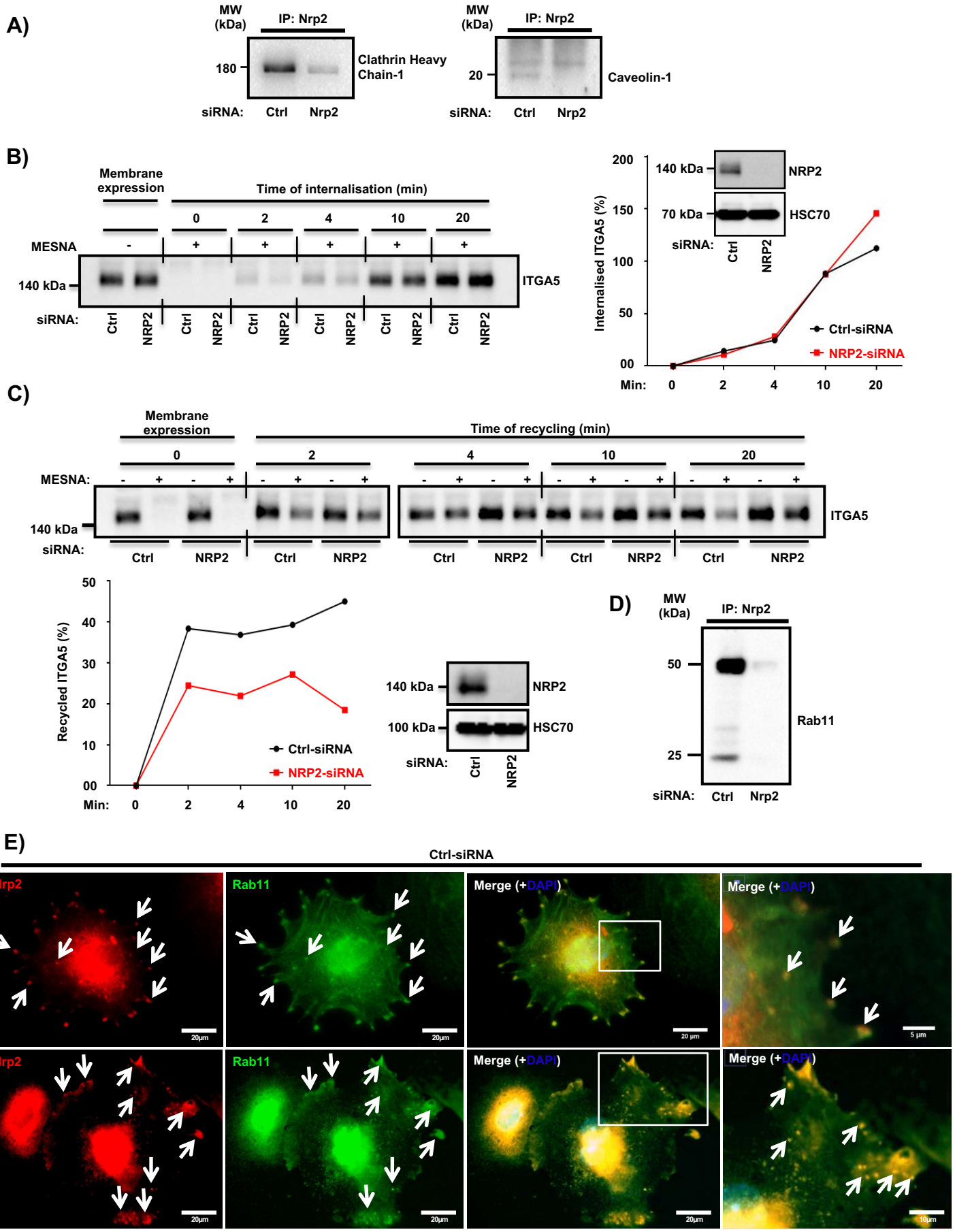
A)
MW (kDa)
IP: Nrp2
180
Clathrin Heavy Chain-1
siRNA: Ctrl Nrp2
MW (kDa)
IP: Nrp2
20
Caveolin-1
siRNA: Ctrl Nrp2
B)
Membrane expression
Time of internalisation (min)
0 2 4 10 20
MESNA
140 kDa
ITGA5
siRNA: Ctrl NRP2
Internalised ITGA5 (%)
140 kDa NRP2
70 kDa HSC70
siRNA: Ctrl NRP2
Ctrl-siRNA
NRP2-siRNA
Min: 0 2 4 10 20
C)
Membrane expression
Time of recycling (min)
0 2 4 10 20
MESNA:
140 kDa
ITGA5
siRNA: Ctrl NRP2
Recycled ITGA5 (%)
Ctrl-siRNA
NRP2-siRNA
Min: 0 2 4 10 20
140 kDa NRP2
100 kDa HSC70
siRNA: Ctrl NRP2
D)
MW (kDa)
IP: Nrp2
50
25
Rab11
siRNA: Ctrl Nrp2
E)
Ctrl-siRNA
Nrp2
Rab11
Merge (+DAPI)
Merge (+DAPI)
20µm
20µm
20 µm
5 µm
Nrp2
Rab11
Merge (+DAPI)
Merge (+DAPI)
20µm
20µm
20µm
10µm

SUPPLEMENTARY FIGURE 1

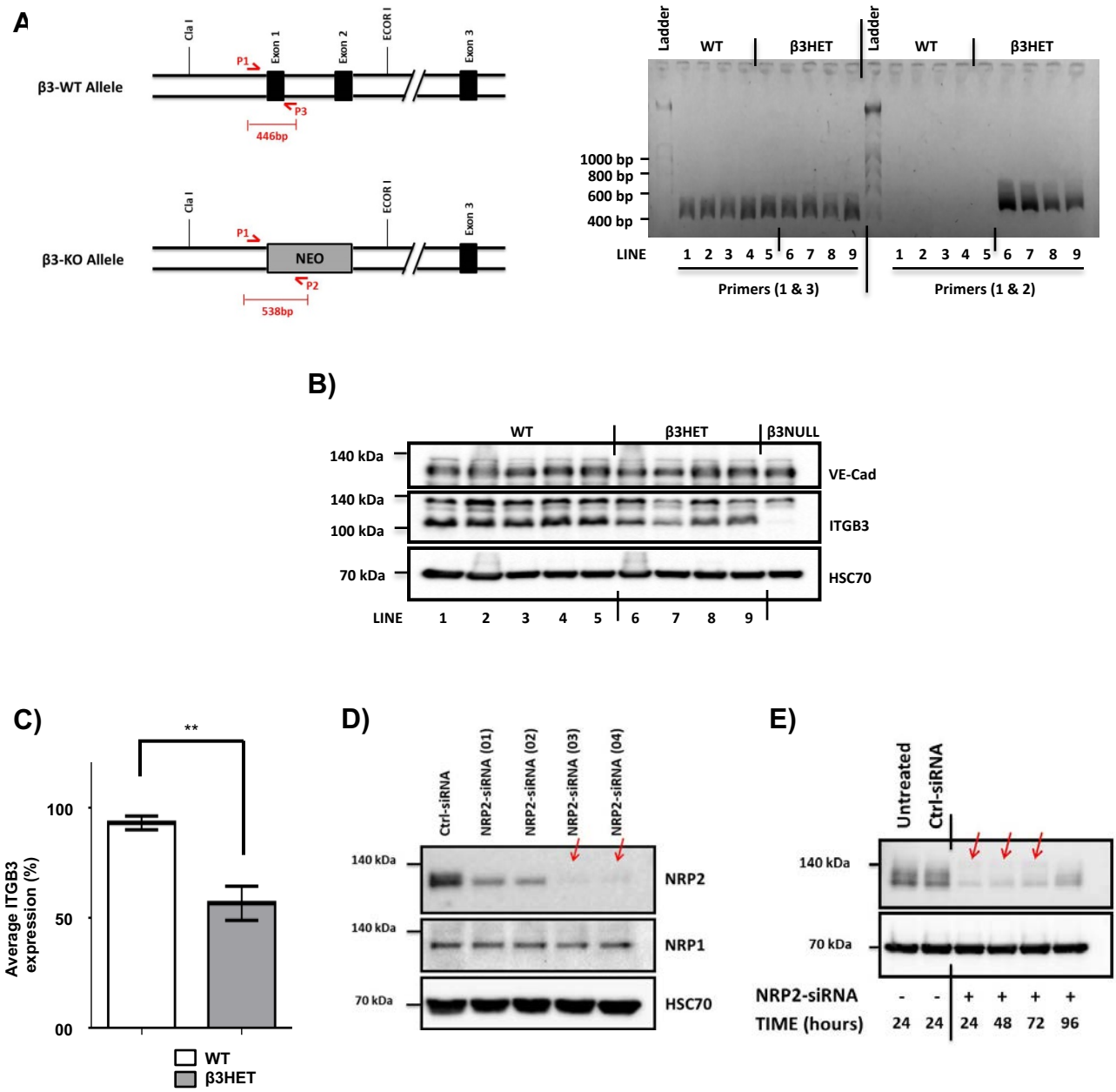

SUPPLEMENTARY FIGURE 2

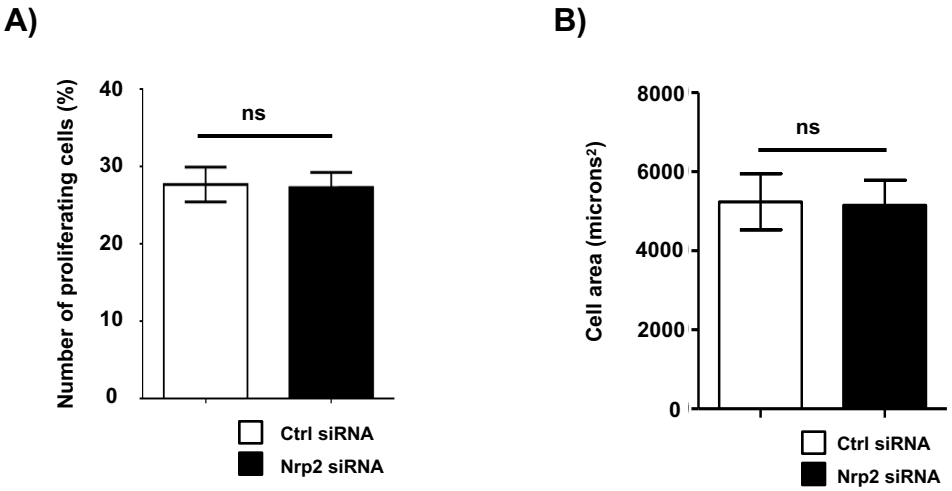

SUPPLEMENTARY FIGURE 3

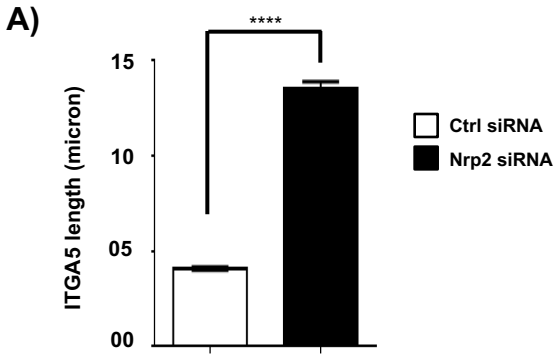

SUPPLEMENTARY FIGURE 4

A)

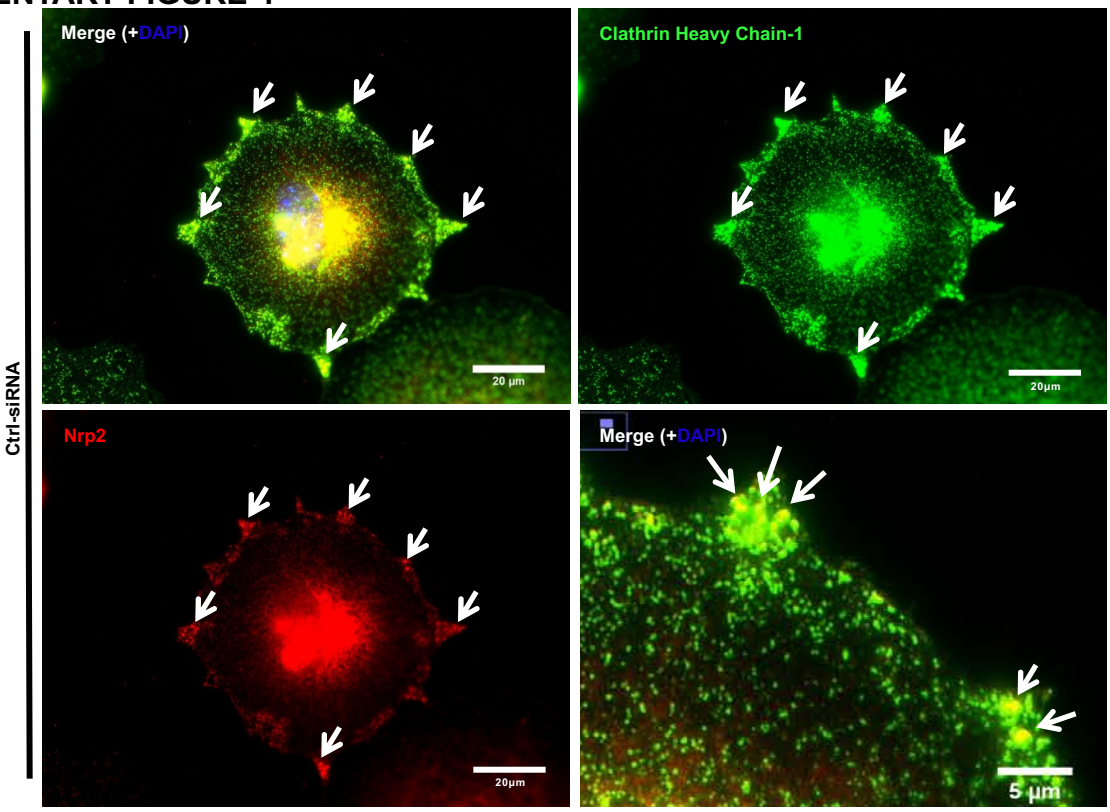

B)

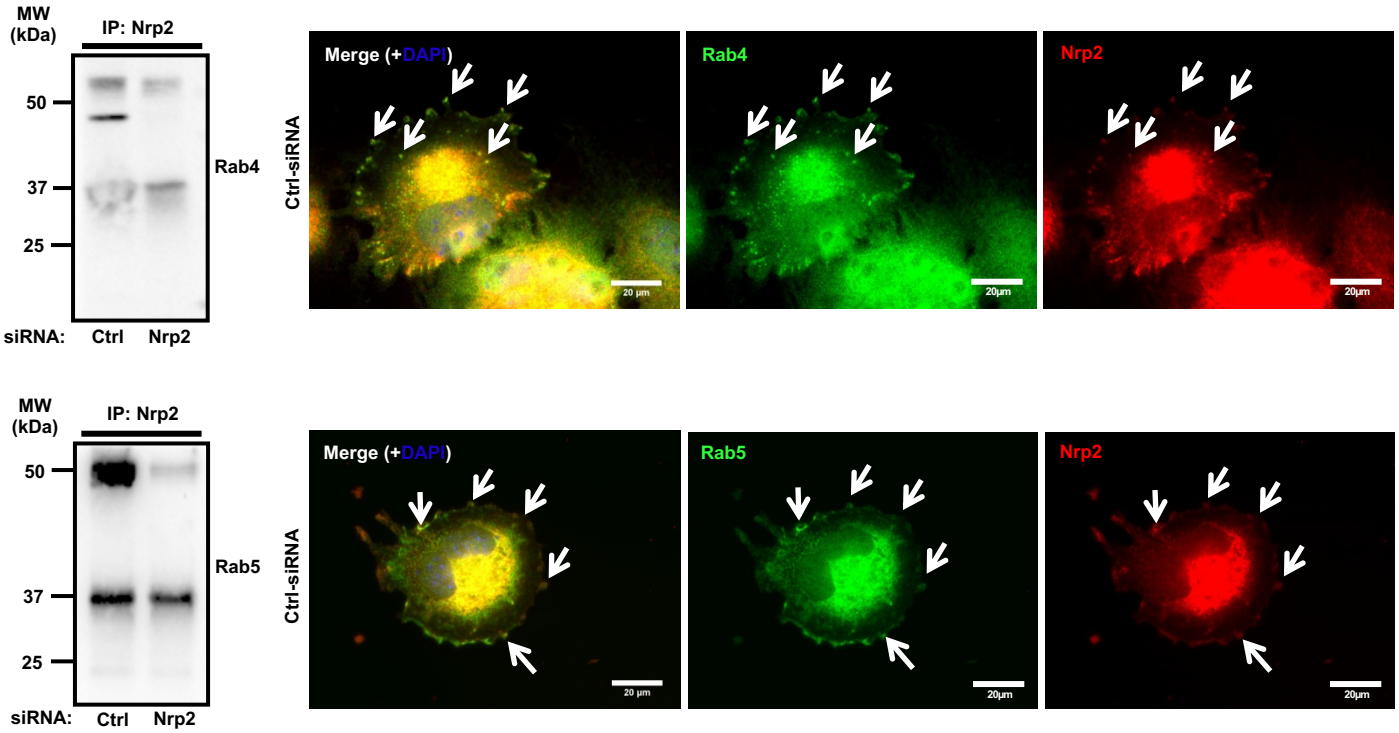

C)

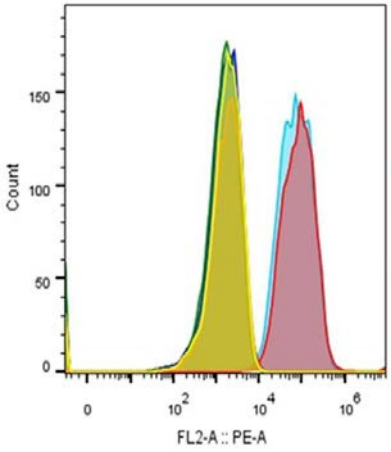

	ECs	Antibody
	Ctrl-siRNA	ITGA5
	NRP2-siRNA	ITGA5
	Ctrl-siRNA	Isotype
	NRP2-siRNA	Isotype
	Ctrl-siRNA	Unstained
	NRP2-siRNA	Unstained